

Для чисельного моделювання аеродинаміки багатоеlementного профілю застосовуються осереднені за Рейнольдсом рівняння Нав'є-Стокса нестисливого середовища, замкнуті однопараметричною диференціальною моделлю турбулентності Spalart-Allmaras. Система вихідних рівнянь записувалася щодо довільної криволінійної системи координат. Узгодження полів тиску і швидкості здійснювалося за допомогою методу штучної стисливості, модифікованого для розрахунку нестационарних задач. Інтегрування системи вихідних рівнянь проводилося чисельно з використанням методу контрольного об'єму. Для конвективних потоків використовувалася протипотокова апроксимація Rogers-Kwak, заснована на схемі Roe третього порядку точності. У моделях турбулентності для апроксимації конвективних складових застосовувалася схема TVD з обмежувачем потоків ISNAS третього порядку. Представлені результати розрахунку турбулентного обтікання багатоеlementного профілю в широкому діапазоні кутів атаки. У результаті проведених досліджень виконано аналіз поля течії навколо багатоеlementного профілю, коефіцієнтів тиску, підняльної сили та сили лобового опору. Виділено фізичні особливості структури течії при обтіканні багатоеlementного профілю ЗОРЗОН. У досліджуваному діапазоні кутів атаки обтікання профілю у злітно-посадковій конфігурації носить стаціонарний характер за винятком областей, де відрив потоку відбувається з гострих кромки, таких як внутрішня частина передкрилки і область в хвостовій частині основного профілю. Усередині цих областей виникають рециркуляційні течії. Зі збільшенням кута атаки розміри відривної зони на внутрішній поверхні передкрилки зменшуються, а в хвостовій частині основного профілю залишаються майже незмінними. На верхній поверхні основного профілю формується струмінь повітря внаслідок прискорення потоку між передкрилкою і передньою кромкою основного профілю. Наявність зазору між основним профілем і задкрилкою призводить до інтерференції струменевих течій на верхній задкрилці. Показано, що злітно-посадкова конфігурація володіє вищими значеннями коефіцієнта підйомної сили, ніж крейсерська конфігурація, особливо на великих кутах атаки. Результати розрахунків задовільно погоджуються з даними інших авторів

Ключові слова: рівняння Нав'є-Стокса, модель турбулентності Spalart-Allmaras, багатоеlementний профіль ЗОРЗОН, чисельне моделювання

Received date 29.07.2019

Accepted date 23.08.2019

Published date 05.10.2019

1. Introduction

Modern aviation equipment for various purposes has widely utilized multi-element airfoils. Composite profiles make it possible, at the current value of an aircraft speed, to reach large values of the wing lifting force under a take-off- and landing mode, maneuvering, or speed deceleration. At the same time, the multi-element airfoils provide for the lower resistance strength values under a horizontal flight mode at cruise altitude [1]. Such values for the aerodynamic characteristics of aviation airfoils are achieved by introducing a slat and a flap into the structure of the wing.

UDC 532.516

DOI: 10.15587/1729-4061.2019.174259

AERODYNAMICS OF THE TURBULENT FLOW AROUND A MULTI-ELEMENT AIRFOIL IN CRUISE CONFIGURATION AND IN TAKEOFF AND LANDING CONFIGURATION

D. Redchys

PhD, Senior Researcher

Department of Dynamics and Strength of

New Types of Transport

Institute of Transport Systems and Technologies of the

National Academy of Sciences of Ukraine

Pysarzhevskoho str., 5, Dnipro, Ukraine, 49005

E-mail: redchits_da@ua.fm

A. Gourjii

Doctor of Physical and Mathematical Sciences, Professor

Department of Automation Design of

Energy Processes and Systems

National Technical University of Ukraine

"Igor Sikorsky Kyiv Polytechnic Institute"

Peremohy ave., 37, Kyiv, Ukraine, 03056

E-mail: a.gourjii@gmail.com

S. Moiseienko

PhD, Associate Professor*

E-mail: 4moiseenko@ukr.net

T. Bilousova*

E-mail: tbbelousovane@gmail.com

*Department of Higher Mathematics and

Mathematical Modeling

Kherson National Technical University

Beryslavske highway, 24, Kherson, Ukraine, 73008

Copyright © 2019, D. Redchys, A. Gourjii, S. Moiseienko, T. Bilousova

This is an open access article under the CC BY license

(<http://creativecommons.org/licenses/by/4.0>)

Conducting aerodynamic wind tunnel tests of full-scale three-dimensional wing configurations, a wing-fuselage system at Reynolds Re numbers corresponding to flight modes, is technically difficult and expensive. Engineering calculations and the results obtained from wind tunnel tests at low Reynolds Re numbers for multi-element airfoils cannot be extrapolated for the Reynolds Re large numbers. A change in air flow speed alters the ratio between the forces of inertia and viscous resistance. This leads not only to a change in the overall flow-around pattern of a wing airfoil, but also to the emergence of significant errors in determining the values for aerodynamic characteristics of aircraft. That is why there

has been a recent increase in interest in numerical modelling of the turbulent flow around the airfoils with high values of the lifting force, at high Reynolds numbers [2–5].

2. Literature review and problem statement

Mathematical modeling of the turbulent flow around multi-element airfoils is a rather difficult task of computational aerodynamics [4, 5]. Many publications in the modern scientific literature attempt to solve this problem [6–13].

Paper [6] reports an experimental study into the flow around the three-element aerodynamic airfoil 30P30N for cruise configuration in the range of Reynolds numbers from 4.6×10^5 to 1.1×10^6 and the angles of attack from 0° to 12° . The authors give the distributed aerodynamic airfoil characteristics. However, there are no general integrated data on the entire three-element airfoil and its individual components.

Work [7] presents experimental and numerical results from studying the aerodynamic and acoustic characteristics of the airfoil 30P30N at a Mach number of 0.17 and the angles of attack from 0° to 8° . The study focused on an acoustic field analysis, the spectral shape of noise, the tonal frequency and location of the noise source. This work did not address the issues related to the integrated and distributed characteristics for the multi-element airfoil at large Reynolds numbers and angles of attack.

Experimental work [8] measured a velocity field around the 30P30N airfoil at $Re=1.2\text{--}1.71 \times 10^6$ and the attack angles of 3° , 5.5° , 8.5° . The authors analyzed the distribution of a pressure factor across the surface of the multi-element airfoil, as well as the acoustic field in the near trail behind the airfoil elements. Work [8] does not address the large angles of attack. Information on such angles is extremely important from the point of view of flight safety. This is due to the fact that at large angles of attack there may occur the air flow detachment from an aircraft wing, which could lead to a sharp drop in the lifting force and, as a result, to stalling the plane in a flat spin.

Paper [9] reports results from a numerical simulation of the 30P30N airfoil's aerodynamics using the RANS-LES hybrid method on multi-block structured and unstructured grids. The authors considered only a single takeoff and landing configuration at a low angle of attack of 5.5° . The cited paper does not provide data on the integrated and distributed characteristics for other angles of attack, nor the cruise configuration of the 30P30N airfoil.

Study [10] gives results from a numerical simulation of the turbulent flow around the 30P30N airfoil at Mach number of 0.17. Only small angles of attack were considered: 4° , 5.5° , 8.5° . The Reynolds number was 1.6×10^6 , which is an order of magnitude less than the values corresponding to actual wings.

Paper [11] made an attempt, based on numerical modeling employing the commercially available software ANSYS Fluent, to manage the structure of the flow around the 30P30N airfoil. The authors considered different slat deviation angles at a fixed attack angle of the main profile. However, the cited paper did not address other airfoil geometric configurations.

Experimental work [12] employed anemometry based on the particles images to investigate the interaction between vortexes that descended from the slat and the boundary lay-

er at the main profile. The study was conducted at low Reynolds numbers of $9.3 \times 10^3\text{--}3.05 \times 10^4$. These results cannot be extrapolated to large Reynolds numbers of the order of 10^7 .

One of the tasks in work [13] to demonstrate the capability of the devised numerical method on structured intersecting grids was to study the structure of the flow around the multi-element airfoil 30P30N. Calculations were performed for the takeoff and landing configuration at a zero angle of attack. The authors gave the pressure factor distribution across the surface of the airfoil. However, the cited work does not provide data on integrated characteristics. In addition, the calculations are given for a single configuration.

Based on our analysis of the scientific literature, one can say that none of the articles reviewed compared the cruise and the takeoff and landing configurations of the multi-element airfoil 30P30N. In addition, all estimated and experimental data refer only for low Reynolds numbers and small angles of attack. All this suggests that it is appropriate to conduct a study on comparing the 30P30N airfoil in the cruise configuration and the takeoff and landing configuration at a large Reynolds number and at a wide range of attack angles.

3. The aim and objectives of the study

The aim of this study is to model mathematically the physical processes at the turbulent flow around the 30P30N multi-element airfoil for the cruise configuration and the take-off and landing configuration over a wide range of attack angles. This would make it possible to investigate the fields of pressure and velocity, the instantaneous lines of current, the surface pressure ratio distribution, as well as values for basic aerodynamic characteristics of the airfoil. Such information is necessary to obtain qualitative assessments of the structure of the flow around the 30P30N airfoil and quantitative values for the aerodynamic forces acting on a wing structure when designing aircraft for different purposes.

To accomplish the aim, the following tasks have been set:

- to state the problem on the turbulent flow around the 30P30N airfoil in the cruise configuration and the takeoff and landing configuration;
- to construct a numerical algorithm to solve the system of initial differential equations;
- to perform numerical modeling, to compare with experimental data, and to identify the physical features of the structure of the flow around a multi-element airfoil over a wide range of angles of attacks.

4. Statement of the problem on the turbulent flow around the 30P30N airfoil in the cruise configuration and in the takeoff and landing configuration

Parameters for the field and computational experiments.

The experimental study into the turbulent flow around the 30P30N multi-element airfoil in the range of attack angles from 0° to 23.4° was conducted by NASA and reported in papers [14, 15]. The three-element airfoil 30P30N (Fig. 1, *a*, *b*) consists of a slat, a main airfoil, and a flap. Two configurations are considered: cruise (configuration *A*) and takeoff and landing (configuration *B*). In the takeoff and landing configuration, the slat and flap are deflected to a 30° angle

relative to the main profile. In the experiment [14, 15], only the takeoff and landing configuration was considered. The Reynolds number, determined based on the profile chord in the folded state and at speed of the unperturbed flow, was $Re=9.0 \times 10^6$.

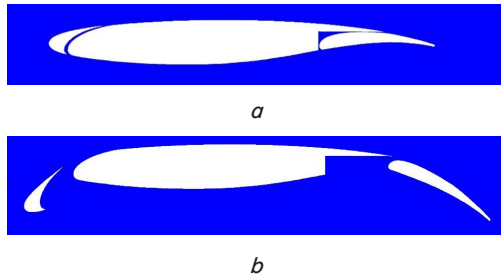


Fig. 1. Configuration of the three-element airfoil 30P30N: *a* – cruise (configuration A); *b* – takeoff and landing (configuration B)

Initial equations. The paper examines the low-speed air movement at small Mach numbers ($M < 0.3$). In this case, the effects of air compression can be neglected; the principal equations that describe the movement of a solid medium are the Reynolds averaged Navier-Stokes equations for a viscous incompressible flow [16].

$$\frac{\partial u_j}{\partial x_j} = 0, \tag{1}$$

$$\frac{\partial u_i}{\partial t} + \frac{\partial(u_j u_i)}{\partial x_j} = -\frac{1}{\rho} \frac{\partial p}{\partial x_i} + \frac{\partial}{\partial x_j} \left[(v + v_t) \left(\frac{\partial u_i}{\partial x_j} + \frac{\partial u_j}{\partial x_i} \right) \right], \tag{2}$$

where $x_i, i=1, 2$ are the Cartesian coordinates; t – time; u_i are the Cartesian components of the velocity vector; p – pressure; ρ – density; v and v_t are the kinematic coefficients of molecular and turbulent viscosity.

Simulation of turbulence. The differential single-parametric Spalart-Allmaras (SA) model is used to close the Reynolds averaged Navier-Stokes equations [17].

The standard Spalart-Allmaras turbulence model is intended to determine the dimensional kinematic coefficient of turbulent viscosity

$$v_t = \tilde{v}_t \cdot f_{v1}, \quad f_{v1} = \chi^3 / (\chi^3 + c_{v1}^3), \tag{3}$$

where f_{v1} is a damping function of kinematic viscosities χ . Here \tilde{v}_t is the working variable. The equation to determine \tilde{v}_t in the Spalart-Allmaras model takes the form [17].

$$\frac{D\tilde{v}_t}{Dt} = c_{b1} \tilde{S} \tilde{v}_t + \frac{1}{\sigma} \frac{\partial}{\partial x_k} \left[(v + \tilde{v}_t) \frac{\partial \tilde{v}_t}{\partial x_k} \right] + \frac{c_{b2}}{\sigma} \frac{\partial \tilde{v}_t}{\partial x_k} \frac{\partial \tilde{v}_t}{\partial x_k} - f_w \left(\frac{c_{b1}}{k^2} + \frac{1 + c_{b2}}{\sigma} \right) \left(\frac{\tilde{v}_t}{d} \right)^2. \tag{4}$$

The first term in the right-hand part of equation (7) is the source term of turbulence generation

$$\tilde{S} \equiv f_{v3} W + \frac{\tilde{v}_t}{k^2 d^2} f_{v2}, \quad W = \sqrt{2W_{ij}W_{ij}}, \tag{5}$$

where W_{ij} is a tensor of swirl.

Function f_{v2} is determined from ratio

$$f_{v2} = 1 - \frac{\chi}{1 + \chi f_{v1}}. \tag{6}$$

The second and third terms in the right-hand part (4) are responsible for the dissipation of turbulence. The fourth one – for the destruction of turbulence near a rigid wall; it contains function

$$f_w = g \left[\frac{1 + c_{w3}^6}{g^6 + c_{w3}^6} \right]^{1/6}. \tag{7}$$

The values for other constants can be found in paper [17].

5. Numerical algorithm for solving the system of initial differential equations

The system of initial equations (1), (2), (4) was recorded with respect to an arbitrary curvilinear coordinate system. The harmonization of pressure and velocity fields was carried out using an artificial compression method, modified to calculate non-stationary problems [18, 19]. The system of initial equations was integrated numerically using the control volume method. The Rogers-Kwak counter-flow approximation, based on the Roe scheme of third-order accuracy, was used for convective terms. In the turbulence model, a TVD scheme with a third-order ISNAS flow limiter was used to approximate the convective terms [20]. Regular grids were used as the baseline to create a discrete analogue of the initial equations. Multi-block computing technologies were used in heterogeneous regions, in which the dimensionality of individual intersecting grids (blocks) is not related. Such an approach has made it possible to devise a unified methodology for calculating the currents within a viscous medium around bodies with a complex geometric shape [21].

6. Results of numerical simulation of the aerodynamics of the three-element airfoil 30P30N

The problem was then nondimensionalized for the characteristic size of the 30P30N airfoil wing section – the chord c and the characteristic velocity U_0 of an unperturbed air flow. Numerical simulation was carried out on the computational grid, which consisted of 19 units with a total of 2.1×10^5 nodes. The thickness of the first layer of the uneven grid, which was closest to a hard surface, was 1.0×10^{-6} . The outer boundary of the estimated area was at a distance of 20 profile's chords. The nodes were condensed in the direction of normal to the surface, as well as to the front and back edges of the profile's elements. To adequately resolve the wall effects in the border layer there were 50...150 layers of the grid towards normal to the surface of the wing. The step of integrating the motion equations of a solid environment was equal to $\Delta t = 0.01$.

The three-element 30P30N airfoil in the cruise configuration performs similarly to a single-cell airfoil. At small angles of attack, the flow around an airfoil is attached in character (Fig. 2, 3, *a, b*), and at angles of 16° and above (a supercritical mode) the flow is detached near the leading edge of the slat (Fig. 2, 3, *c*).

Numerical modeling shows that in the examined range of angles of attack the airfoil is flowed around in the takeoff and landing configuration in a quasi-stationary fashion. Specifically, for the angle of attack of 0°, the current pattern is characterized by a continuous mode, except for the regions areas where the flow is detached from sharp edges (the inner part of the slat and the region in the tail part of the main profile). There are the recirculation currents within these areas. Fig. 4, *a* illustrates the distribution of current lines and pressure fields in the region adjacent to the wing; Fig. 5, *a* shows the distribution of the speed module when the three-element 30P30N airfoil is flown around. As the angle of attack increases, the size of the detachable zone at the inner surface of the slat decreases (Fig. 5, *b, c*); while it remains almost constant in the tail part of the main profile.

At the angle of attack of 8.1°, the flow detachment is observed near the rear edge of the flap. This is evidenced by the distribution of a pressure factor (Fig. 6, *b*). The figures show the dependence of pressure factor on the relative coordinate of the wing chord. Fig. 5, *c* (the angle of attack is 23.4°) clearly shows an air jet formed at the upper surface of the main profile.

The distribution of pressure factor across the surface of the profile for the angles of attack $\alpha=0^\circ, 8.1^\circ, 23.4^\circ$ are shown in Fig. 6. Coefficients for the lifting force and the drag force are determined from the following expressions

$$C_L = \frac{F_y}{\rho U_0^2 S}, \quad C_D = \frac{F_x}{\rho U_0^2 S}, \quad (8)$$

where F_x and F_y are the projections of aerodynamic forces onto the axes of the Cartesian coordinates, S is the surface area of the wing. The values for these coefficients depend on the wing profile, airflow speed U_0 , and angle of attack α . Fig. 7 shows dependences of values for the lifting force coefficient and the drag coefficient on values for the angle of attack of the 30P30N wing airfoil. The obtained results are in satisfactory agreement with the experimental data.

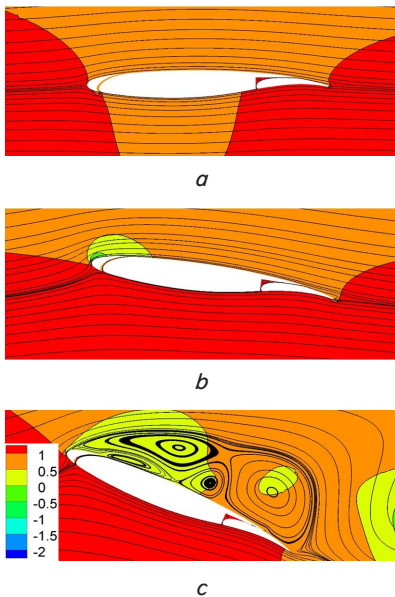


Fig. 2. Instantaneous lines of current and a pressure field isolines (configuration A): $a - 0^\circ$; $b - 8.1^\circ$; $c - 23.4^\circ$

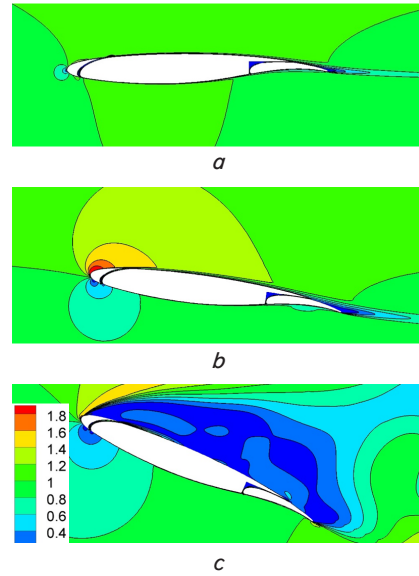


Fig. 3. Speed module isolines (configuration A): $a - 0^\circ$; $b - 8.1^\circ$; $c - 23^\circ$

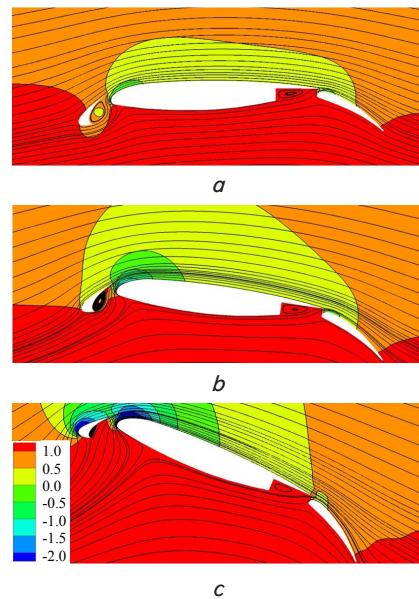


Fig. 4. Instantaneous lines of current and a pressure field isolines (configuration B): $a - 0^\circ$; $b - 8.1^\circ$; $c - 23.4^\circ$

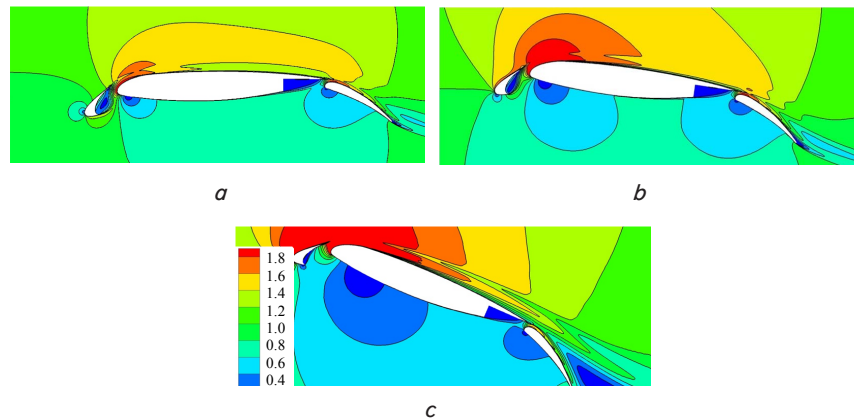


Fig. 5. Speed module isolines (configuration B): $a - 0^\circ$; $b - 8.1^\circ$; $c - 23.4^\circ$

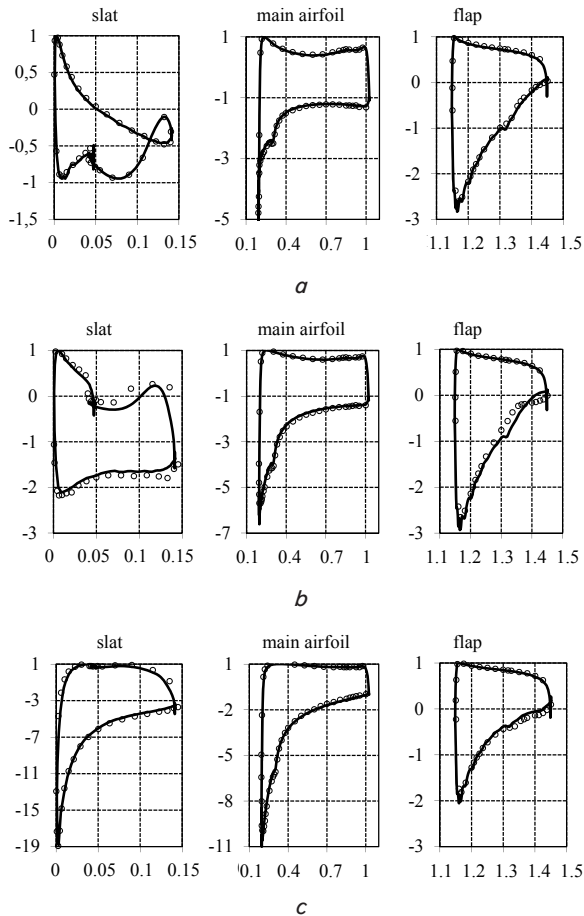


Fig. 6. Distribution of pressure factor across the airfoil surface (configuration B) at angles of attack: $a - 0$; $b - 8.1$; $c - 23.4$ (○ – experiment [14]; — – current work)

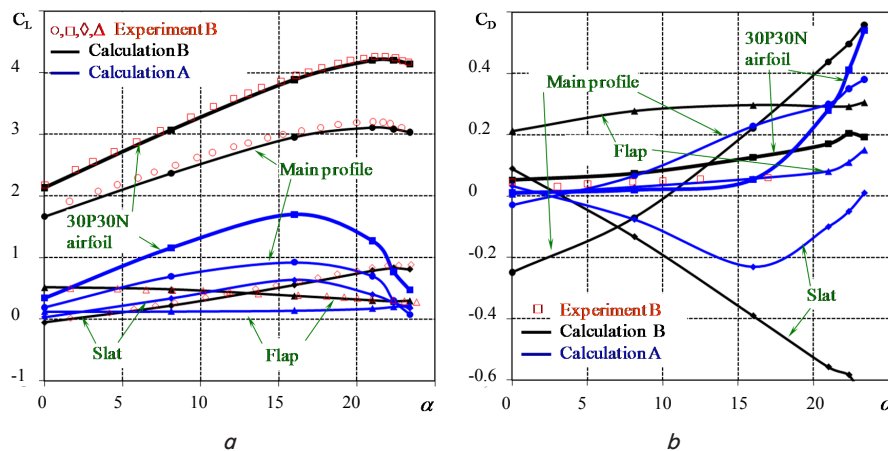


Fig. 7. Dependence of aerodynamic coefficients on angle of attack: $a -$ lifting force; $b -$ drag force (○, □, ◇, Δ – experiment [14]; — – current work)

7. Discussion of results of modeling numerically the 30P30N airfoil aerodynamics

In general, flow around a three-element airfoil is characterized by complex physical processes. These include the viscous-non-viscous interaction between flows coming off the outer surface of the slat and passing into the gap between the slat and the leading edge of the main profile. Fig. 5, c clearly

shows a jet of air formed at the top surface of the main profile. The formation of this jet is due to the acceleration of the flow between the slat and the spout of the main profile. The presence of a gap between the main profile and the slat leads to the interference of jet currents at the top surface of the slat. The air flow coming down from the top surface of the main profile presses the flow that passes through the gap between the main profile and the slat to the outer surface of the latter. The formation of this type of jet current is explained by that the flow coming down from the upper surface of the main profile has a lower speed and, therefore, a greater pressure, which is implemented by pressing the flow that passes through the gap to the outer surface of the slat. This results in a detachment-free mode of flowing around a multi-element airfoil at angles at which detachment would occur for a single profile.

When configuration A is flown around at large angles of attack (Fig. 3, c), the air flow is no longer able to push through the increasing pressure gradient at the upper leeward side of the profile and there is a flow detachment, which leads to a drop in the lifting force coefficient. As the angle of attack increases, this detachable zone increases. Configuration B demonstrates the higher values for the lifting force coefficient than those for configuration A, especially at large angles of attack.

The results obtained are in good agreement with existing physical understanding of the Coanda effect, according to which a jet incident to the curvilinear surface sucks the air near a rigid surface and creates rarefaction that presses the jet to the profile surfaces. Owing to this, a multi-element airfoil is flown around without detaching the flow from the bearing surfaces (Fig. 4, 5), except for small angular vortexes in the regions of structural junction between the slat and the flap and the main profile.

The quality of results obtained is ensured by the use of fundamental models of a continuous medium, by high quality of modern modeling of turbulent currents. The proposed numerical algorithm makes it possible to perform effective calculations for the bodies of different geometry that are flown around by high-speed streams of gas and liquid.

Further research should include accounting for the three-dimensional effects on the airfoil aerodynamics, the optimization of the aerodynamic shape of the airfoil in order to improve the aerodynamic quality of an aircraft's wing under different speed motion modes.

7. Conclusions

1. We have stated the problem on the turbulent flow around the multi-element airfoil 30P30N.

The initial equations for the dynamics of a viscous incompressible medium have been recorded, closed by a single-parametric differential model of turbulence. We have constructed a computational grid around the 30P30N airfoil for the cruise configuration and the takeoff and landing configuration at angles of attack of 0° , 8.1° , 23.4° .

2. A numerical algorithm has been constructed for solving the system of the initial Navier-Stokes differential equations, as well as the Spalart-Allmaras turbulence model, to

solve the set problem. The system of initial equations was integrated numerically using the control volume method. The Rogers-Kwak counter-flow approximation of third-order accuracy was used for convective terms. In the turbulence model, a TVD scheme with a third-order ISNAS flow limiter was used to approximate the convective terms.

3. We have performed numerical simulation of flow around the 30P30N airfoil at the Reynolds number of 9.0×10^6 . The physical features of the current structure have been identified. It has been established that an increase

in the angle of attack leads to a decrease in the size of the detachable zone at the inner surface of the slat; in the tail part of the main airfoil, it remains almost constant. It has been shown that values for the 30P30N airfoil lifting force coefficient in the takeoff and landing configuration are two to five times higher than those in the cruise configuration. The results obtained were compared with experimental data. The calculations results are in satisfactory agreement with the experimental data. The discrepancy does not exceed 10 per cent.

References

1. Smith, A. M. O. (1975). High-Lift Aerodynamics. *AIAA*, 12 (6), 501–530.
2. Lin, J. C., Robinson, S., McGhee, R. J. (1992). Separation control on high Reynolds number multielement airfoils. *AIAA*, 2 (2), 45–66.
3. Anderson, W. K., Bonhaus, D. L., McGhee, R. J., Walker, B. S. (1995). Navier-Stokes computations and experimental comparisons for multielement airfoil configurations. *Journal of Aircraft*, 32 (6), 1246–1253. doi: <https://doi.org/10.2514/3.46871>
4. AGARD CP-515. High-lift aerodynamics. Proceedings of the 71st AGARD FDP Symposium on High-Lift Aerodynamics (1993). Banff, 513.
5. Proceedings of the fifth Symposium on Numerical and Physical Aspects of Aerodynamic Flows (1992). Long Beach, CA, USA, 474.
6. Kamliya Jawahar, H., Azarpeyvand, M., Ilario, C. (2017). Experimental Investigation of Flow Around Three-Element High-Lift Airfoil with Morphing Fillers. 23rd AIAA/CEAS Aeroacoustics Conference. doi: <https://doi.org/10.2514/6.2017-3364>
7. Li, L., Liu, P., Guo, H., Hou, Y., Geng, X., Wang, J. (2017). Aeroacoustic measurement of 30P30N high-lift configuration in the test section with Kevlar cloth and perforated plate. *Aerospace Science and Technology*, 70, 590–599. doi: <https://doi.org/10.1016/j.ast.2017.08.039>
8. Pascioni, K., Cattafesta, L. N., Choudhari, M. M. (2014). An Experimental Investigation of the 30P30N Multi-Element High-Lift Airfoil. 20th AIAA/CEAS Aeroacoustics Conference. doi: <https://doi.org/10.2514/6.2014-3062>
9. Ashton, N., West, A., Mendon a, F. (2016). Flow Dynamics Past a 30P30N Three-Element Airfoil Using Improved Delayed Detached-Eddy Simulation. *AIAA Journal*, 54 (11), 3657–3667. doi: <https://doi.org/10.2514/1.j054521>
10. Gao, J., Li, X., Lin, D. (2017). Numerical Simulation of the Noise from the 30P30N Highlift Airfoil with Spectral Difference Method. 23rd AIAA/CEAS Aeroacoustics Conference. doi: <https://doi.org/10.2514/6.2017-3363>
11. Tang, G., Agarwal, R. K. (2018). Active Control of Flow Over a Three-Element Airfoil in Unbounded Flow and Ground Effect. 2018 AIAA Aerospace Sciences Meeting. doi: <https://doi.org/10.2514/6.2018-0791>
12. Wang, J., Wang, J., Kim, K. C. (2018). Wake/shear layer interaction for low-Reynolds-number flow over multi-element airfoil. *Experiments in Fluids*, 60 (1). doi: <https://doi.org/10.1007/s00348-018-2662-5>
13. Xu, J., Cai, J., Liu, Q., Qu, K. (2014). Flow Simulations by Enhanced Implicit-Hole-Cutting Method on Overset Grids. *Journal of Aircraft*, 51 (5), 1401–1409. doi: <https://doi.org/10.2514/1.c032283>
14. Valarezo, W. O., Dominik, C. J., McGhee, R. J., Goodman, W. L. (1992). High Reynolds number configuration development of a high-lift airfoil. AGARD meeting in high-lift aerodynamics.
15. Chin, V., Peters, D., Spaid, F., McGhee, R. (1993). Flowfield measurements about a multi-element airfoil at high Reynolds numbers. 23rd Fluid Dynamics, Plasmadynamics, and Lasers Conference. doi: <https://doi.org/10.2514/6.1993-3137>
16. Anderson, J. (1995). *Computational Fluid Dynamics*. McGraw-Hill Education, 576.
17. Rogers, S., Kwak, D. (1988). An upwind differencing scheme for the time-accurate incompressible Navier-Stokes equations. 6th Applied Aerodynamics Conference. doi: <https://doi.org/10.2514/6.1988-2583>
18. Rogers, S. E., Kwak, D. (1990). Upwind differencing scheme for the time-accurate incompressible Navier-Stokes equations. *AIAA Journal*, 28 (2), 253–262. doi: <https://doi.org/10.2514/3.10382>
19. Rogers, S. E., Kwak, D. (1991). An upwind differencing scheme for the incompressible Navier-Stokes equations. *Applied Numerical Mathematics*, 8 (1), 43–64. doi: [https://doi.org/10.1016/0168-9274\(91\)90097-j](https://doi.org/10.1016/0168-9274(91)90097-j)
20. Zijlema, M. (1994). On the construction of third-order accurate TVD scheme using Leonards normalized variable diagram with application to turbulent flows in general domains. Technical Report DUT-TWI-94-104, 25.
21. Redchits, D. A. (2009). Mathematical modelling of separated flows on the basis of unsteady Navier-Stokes equations. *Nauchnye vedomosti Belgorodskogo gosudarstvennogo universiteta. Seriya: Matematika. Fizika*, 13 (68), 118–146.